Clays and Clay Minerals, Vol. 57, No. 1, 54–71, 2009.

HYDROGEN BONDING AND VIBRATIONAL SPECTRA IN KAOLINITE-DIMETHYLSULFOXIDE AND -DIMETHYLSELENOXIDE INTERCALATES – A SOLID-STATE COMPUTATIONAL STUDY

EVA SCHOLTZOVÁ* AND L'UBOMÍR SMRČOK

Institute of Inorganic Chemistry, Slovak Academy of Sciences, Dúbravská cesta 9, SK-845 36 Bratislava, Slovak Republic

Abstract—The aims of this study were to obtain accurate structural information on the dimethyl sulfoxide (DMSO) and dimethylselenoxide (DMSeO) kaolinite intercalates, paying close attention to the hydrogen-bond geometries, and to provide a detailed interpretation of the individual vibrational modes of intercalates under study and relate their energies to the formation of the hydrogen bonds. Accurate positions of all the atoms in the structures of kaolinite:dimethylsulfoxide (K:DMSO) and kaolinite:dimethylselenoxide (K:DMSeO) intercalates have been obtained by the total energy minimization in solid state at density functional theory (DFT) level of the theory. The bond distances and angles in the kaolinite 1:1 layer are in good agreement with those reported in the most recent single-crystal refinement of kaolinite. Computed geometries of DMSO and DMSeO agree well with the high-quality diffraction data and independent theoretical *ab initio* calculations. The organic molecules are fixed in the interlayer space mainly by three moderately strong O–H···O hydrogen bonds, of different strengths, with the O···O contact distances being within 2.739–2.932 Å (K:DMSO) and 2.681–2.849 Å (K:DMSeO). Substantially weaker C–H···O and O–H···S(Se) contacts play only a supporting role. The optimized atomic coordinates were used to calculate the individual vibrational modes between 0 and 4000 cm^{-1}. The maximum red shifts of the OH-stretching modes caused by the formation of the O–H···O hydrogen bonds were 407 cm^{-1} (K–DMSO) and 537 cm^{-1} (K-DMeSO), respectively. The Al–O–H bending modes are spread over the large interval of 100–1200 cm^{-1}, but the dominant contributions are concentrated between 800 and 1200 cm^{-1}. Theoretically calculated energies of the OH- and CH-stretching modes show good agreement with the previously published figures obtained from the infrared and Raman spectra of these intercalates.

Key Words—DMSeO, DMSO, DFT, Hydrogen Bonds, Kaolinite, Vibrational Spectra.

INTRODUCTION

Intercalates of phyllosilicates and organic compounds are of interest due to an increasing number of practical applications. Because the macroscopic properties reflect the microscopic structure, knowledge of the crystal and electronic structures is essential in tailoring the materials to meet future requirements. Unfortunately, research on the electronic structures of phyllosilicates is hampered by the large variability in their chemical composition and especially by the frustrating lack of well-ordered single crystals of a sufficient size. With the advent of synchrotron-based techniques, the size of the crystals is slowly becoming less of a problem but the structural disorder inherent in this family of minerals remains.

The lack of the relevant structural information on phyllosilicates available from diffraction or spectral experiments has led to the migration of the various computational methods to the field of structural mineralogy. The main advantage of the computational approach is that, in contrast to XRD, the contributions of the atoms to the total electron density distribution are not weighted by their scattering powers. Moreover, the accuracy of the current computational methods has reached such a level that they can compete with neutron diffraction experiments in obtaining accurate geometries for hydrogen bonds. The additional benefit brought by theoretical calculations is that they not only provide accurate atomic coordinates, but can routinely supply vibrational density of states or even vibrational spectra. The calculated energies of the individual vibrational modes can be reconciled with those observed experimentally and the origins of the latter explained in detail (see *e.g.* Balan *et al.*, 2001, 2002). The most limiting factor in the application of the computational methods is the availability of a reliable initial structural model, and this is the case for most of the phyllosilicates. In the case of organic intercalates, the problem is even more complex as the positions of the atoms in organic molecules are often only estimated by the standard diffraction and/or spectroscopic methods. Moreover, even if the structure is known in sufficient geometric detail, problems still arise because of isomorphous replacement in the cation positions typical in 2:1 layer silicates. A problem with the computational methods is caused by the size of the computational cells; the addition of extra variable elements makes them too large for the computational resources available. Given these issues, intercalates of the 1:1 phyllosilicates are easiest

* E-mail address of corresponding author:
uacheva@savba.sk
DOI: 10.1346/CCMN.2009.0570106

to deal with; with the exception of the cronstedtites, these are not prone to cation substitution and several intercalate structures have already been analyzed by standard physico-chemical methods.

Inasmuch as the basic building units of the kaolinite structure, *i.e*. 1:1 layers, are held by moderately strong O-H···O hydrogen bonds, the interlayer region is, under normal conditions, easily accessible only by a small group of intercalation compounds such as highly polar molecules or salts (Olejnik *et al*., 1970). For many years, attention has been focused on one member of this exclusive group, the kaolinite:dimethylsulfoxide (K:DMSO) intercalation complex, probably because of its relative structural and chemical simplicity and ease of preparation. The DMSO molecule is highly polar: its dipole moment is ~4D; and it is a good proton acceptor and can, optionally, donate to hydrogen bonds the hydrogen atoms from its two methyl groups.

The structure and properties of K:DMSO (Figure 1) have been studied extensively by several physico-chemical methods. The landmark in structural research of the K:DMSO and of kaolinite:dimethylselenoxide (K:DMSeO) intercalates was the study by Raupach, Barron, and Thompson (1987, hereafter RBT) who examined the crystal structures of both intercalates in detail using a combination of powder XRD, infrared (IR) spectroscopy, and nuclear magnetic resonance (NMR) spectroscopy. The study was an extension of previous work by Thompson and Cuff (1985), discussing in detail the crystal structure of the K:DMSO refined from X-ray and neutron powder diffraction data. The paper by Thompson and Cuff (1985) also detailed the strategy used in the structure refinements, based on the 'cyclic' application of structure-factor extraction from powder data, followed by the standard, single-crystal refinement. In addition, the IR and NMR data were exploited in order to obtain some supporting geometrical information for setting up the constrained structure refinement carried out in the *C*1 space group. However, in spite of all the effort, the analysis of the refined structures revealed that the RBT refinements have provided rather unrealistic geometries of the constituting polyhedra, *i.e*. SiO_4 tetrahedra and AlO_6 octahedra. For instance, in the K:DMSO structure, the values of the Si−O bond distances in the tetrahedra varied over the unacceptably wide interval of <1.48, 1.78> Å. In the case of K:DMSeO the interval was similar, but estimates of the bond distances were shifted toward higher values (<1.58, 1.83> Å). The expected value for kaolinite, derived from the most recent single-crystal study, are within the interval 1.605(3)−1.628(3) Å (Neder *et al.*, 1999). (Because no bond distances/angles in the polyhedra are given in the RBT study, they were calculated in the present study using *PLATON* (Spek, 2002), taking the atomic coordinates from table 1 of the RBT paper.)

Although the scatter of the Al−O bond distances in the individual octahedra is less pronounced, extreme values do exist. No doubt, this is a result of the small amount of information extractable from the powder XRD patterns of the low-symmetry compounds influenced by preferred orientation and structural disorder (Smrčok, 1995). However, the accuracy of the atomic coordinates

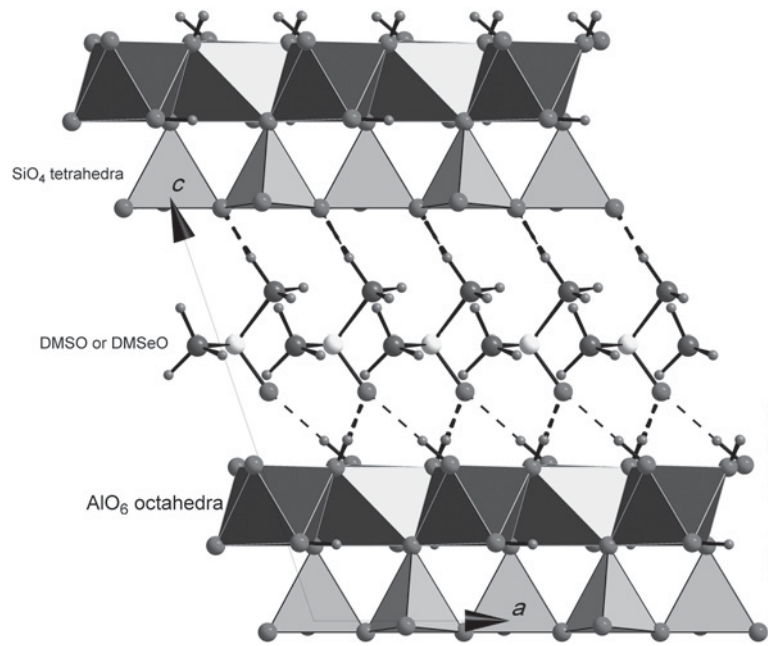

Figure 1. Schematic presentation of the structure of kaolinite intercalated by DMSO (DMSeO) viewed along the *b* axis. Hydrogen bonds are indicated by the dashed lines. Figures 1−4 have been prepared using the *DIAMOND* program of Brandenburg (2006).

has been sufficient to reveal that the organic molecules are locked to the OH layer by the hydrogen bonds through the oxygen atom of the O−S(Se) bond and that the methyl groups interact, by some means, with the basal oxygen atoms of the adjacent 1:1 kaolinite layer.

The suggestion that DMSO molecules hydrogen bond to the hydroxyl layer has also been promoted by several IR and Raman studies. Olejnik *et al.* (1968) suggested that intercalation of DMSO into kaolinite, dickite, and halloysite results from breaking the interlayer hydrogen bonds and reforming them with itself. That proposal was based solely on the appearance of new peaks in the IR spectra at 3568, 3535, and 3499 cm^{-1}, assigned to the OH-stretching vibrations. Later, but still before the RBT paper appeared, Johnston *et al.* (1984) unambiguously identified the stretching vibration attributable to the inner OH group (3620 cm^{-1}) as it was passing uninfluenced from the spectrum of a pure kaolinite to the spectra of various K:DMSO complexes. Those authors also outlined the structure of the intercalated kaolinite, where the DMSO molecules are rotated by 90º compared to their positions in the RBT structure. The presence of the intercalated molecules in the structure was demonstrated by the two rather broad peaks centered at 3538 and 3502 cm^{-1}, the positions of which agree well with the positions of the maxima given by Olejnik *et al.* (1968). From analysis of the energy region between 2850 and 3100 cm^{-1}, Olejnik *et al.* (1968) concluded that two distinct types of CH bonds are present in the structure. More recently, Frost *et al.* (2000) identified, for DMSO-intercalated low-defect kaolinite three 'inner surface' OH-stretching modes at 3660, 3356, and 3501 cm^{-1} at 298 K.

(To avoid difficulties with the terminology, the 'inner' OH groups are assumed here to be those that point toward the center of the ditrigonal cavity, while the 'inner-surface' (also called 'outer') OH groups are, in the untreated structure, hydrogen bonded to the basal oxygen atoms of the adjacent 1:1 layer.)

Upon cooling to 77 K the band at 3660 cm^{-1} split into two bands at 3658 and 3663 cm^{-1} and the energy of the inner hydroxyl mode decreased from 3620 cm^{-1} to 3615 cm^{-1}. In a study of the intercalation of kaolinite with deuterated DMSO (Martens *et al.*, 2002), a new interpretation of the modes falling in a typical region of the hydroxyl-stretching modes, which is based on the presence of water in the structure of the intercalate, was presented. Martens *et al*. (2002) claimed evidence of two types of intercalated water and of two types of DMSO molecules in the structure. In addition to the photon spectroscopies, the dynamics of the DMSO molecules intercalated in the kaolinite interlayer were studied by MAS NMR between 300 and 380 K using ^{13}C and ^{2}H isotopes (Hayashi, 1995, 1997). Two inequivalent methyl groups were identified, one keyed to the ditrigonal hole in the tetrahedral sheet and one rotating freely, which is in line with the methyl-group positions in the RBT model. The activation energy for the keyed-group rotation was estimated to be 13 kJ/mol, while for the unkeyed group, it was only slightly larger at 16.5 kJ/mol, values which were later corroborated by Michalková and Tunega (2007), who established values of 13 kJ/mol and 15.2 kJ/mol through their simulation calculations. Interestingly, the molecular dynamics calculations, carried out using the empirical 6−12 interatomic potentials, predicted the existence of an, as yet, unproven K:DMSO intercalate with $d_{001} \approx 15.3$ Å having two layers of organic molecules within the interlayer region (Fang *et al.*, 2005).

The aims of the present study, based on the application of the solid-state DFT method, are twofold: firstly, to obtain accurate structural information on the DMSO and DMSeO kaolinite intercalates, paying close attention to the hydrogen-bond geometries; and secondly, to provide a detailed interpretation of the individual vibrational modes of intercalates under study and relate their energies to the formation of the hydrogen bonds. The main tool used in this analysis are vibrational densities of state, both total and partial. Although the intensities of such spectra are not directly comparable to those obtained by photon spectroscopies, in conjunction with the calculated vibrational energies (eigenvalues) and eigenvectors describing the directional properties of the individual vibrations, they provide a better insight into the nature of the vibrational processes.

COMPUTATIONAL DETAILS

Inasmuch as intercalation carried out under standard conditions is probably never complete, two idealized computational models assuming full (F) and half (H) occupation of the expected positions of the organic molecules in the structures were proposed. Thus, the intention was to study the influence of the formation of hydrogen bonds on the vibration modes of the OH groups and to clarify the possible impact of the mutual interactions of the neighboring organic molecules on their orientations in the structures. More complicated patterns of the intercalated molecules requiring much larger computational cells and hence very time-demanding calculations were not examined. The computational cells of the K:DMSO ($Si_4Al_4O_{18}H_8{-}C_4S_2H_{12}$) and K:DMSeO ($Si_4Al_4O_{18}H_8{-}C_4Se_2H_{12}$) were based on the atomic coordinates taken from the RBT study. From the suite of K:DMSeO intercalates, the structure labeled 11.26 Å was chosen, because it was claimed by the RBT authors to be the best ordered among those analyzed.

The initial positions of the hydrogen atoms in the methyl groups were estimated, assuming the idealized geometry of the groups, while the hydrogen atoms belonging to the hydroxyl groups were positioned ~1 Å above or below the parent oxygen atoms. The full list of atoms in the F model was then obtained by the expansion of the structure described in the *C*-centered cell to the

primitive cell (*P*1) with identical cell parameters. In the H model, the molecule generated in the original structure by the translation dictated by *C*-centering was omitted.

The calculations were performed using the computer code *VASP* (Kresse and Hafner, 1993; Kresse and Furthmüller, 1996a, 1996b). The exchange-correlation function was expressed in the localized density approximation (LDA) according to Perdew and Zunger (1981), together with the generalized gradient approximation (GGA; Perdew and Wang, 1992). Plane waves formed a basis set and calculations were performed using the projector-augmented wave method (Blöchl, 1994; Kresse and Joubert, 1999) and atomic pseudo-potentials (Kresse and Hafner, 1994). The energy cutoff controlling the accuracy of the calculation was set to 500 eV, representing an extended basis set and consequently highly accurate calculations. The optimizations of the structures were achieved by means of conjugated gradient method in 4*k*-points (Teter *et al.*, 1989; Bylander *et al.*, 1990). All calculations were performed with fixed-cell parameters and all atomic coordinates were allowed to vary. Normal modes of vibrations were calculated within the computational cells from the normal mode analysis accomplished in the frames of the harmonic approximation. The total energy converged to 10^{-7} eV and residual forces on the atoms were <0.0005 eV/Å. The Hessian was constructed from the single-point energy calculations of the 6*n* structures generated from the optimized structures by displacing each of the *n* atoms in the cell in the positive and negative senses along the Cartesian directions *x*, *y*, and *z* (Hafner, 2003). The basis of the method was also described by Kirkpatrick *et al*. (2005). Geometrical analysis of the optimized structures was done by means of the *PLATON* program (Spek, 2002).

RESULTS AND DISCUSSION

Bond distances, angles, orientation of the molecules

The optimized atomic coordinates, bond distances and angles in the kaolinite 1:1 layers are summarized in Tables 1 and 2 (deposited on The Clay Minerals Society website: www.clays.org/journal/JournalDeposits.html). The bond distances and angles in the constituent polyhedra of the kaolinite 1:1 layers (Table 2, deposited on The Clay Minerals Society website: www.clays.org/journal/JournalDeposits.html) are in good agreement with those reported in the most recent single-crystal refinement of kaolinite (Neder *et al.*, 1999) and with the values previously obtained by the total energy minimization in the solid state by another computational method (Hobbs *et al.*, 1997). A comparison of the optimized bond lengths and angles in the DMSO and DMSeO molecules with those derived from the diffraction experiments and the diverse calculations (Table 3, deposited on The Clay Minerals Society website: www.clays.org/journal/JournalDeposits.html) showed that the accuracy of all the computational methods is good, taking the molecular geometries determined in the diffraction experiments (Ibberson, 2005; Filatov *et al.*, 2005) as the reference. The small differences in the geometries of the molecules optimized in the structures of the kaolinite intercalates *vs*. those optimized in the molecular crystals can be attributed to their different environments. The only gross errors in Table 3 (deposited on The Clay Minerals Society website: www.clays.org/journal/JournalDeposits.html) are the values of the Se=C2 bond distance and the C1−Se−C2 bond angle determined in the RBT study. Such inaccuracies are frequent in powder XRD structure refinements and result primarily from the nature of the experiment (Smrčok, 1995). The orientation of the organic molecules sandwiched between the adjacent 1:1 kaolinite layers is limited by the interplay of the hydrogen bonds and orientation of the highly polarized S(Se)=O σ-bond (Dobado *et al.*, 1999) with respect to the local electric field. Taking the plane fit through the O12−O14 hydroxyl oxygen atoms as the reference, the S=O9 bond is inclined at 55º and 52º for the F and H models, respectively. The S−C2 bond is thus almost parallel to the reference plane as the respective angles are only 1º (F) and 2º (H). For the K:DMSeO, a very similar orientation of the molecule was obtained as the values of the respective angles are 49º/52º and 1º/1º. These values are comparable with ~40º (K:DMSO) and ~39º (K:DMSeO) estimated from the RBT study using spectroscopic data. For all the methyl groups the tetrahedral geometry was calculated with the H−C−H bond angles varying between 107 and 112º.

The absence of half of the intercalated molecules, as modeled by the H model, caused only small displacements and tilts of the remaining 50% in the structure compared to their initial positions in the F model. For the purpose of this study, the differences in the positions of the molecules in the F and H models are best expressed by the distances between the corresponding atoms (Figure 2). Generally, the most stable are the positions of the O9 atoms, which are partially fixed by the three O−H···O hydrogen bonds. In the K:DMSO intercalate the O9(F)−O9(H) distance is negligible, ~0.05 Å. In the K:DMSeO it is approximately twice as large, 0.12 Å, but still not worth further consideration. This is not the case, however, for the C(F) and C(H) atoms, which in K:DMSO are separated by ~0.2, or even ~0.3−0.5 Å in the K:DMSeO. While in the K:DMSO structure all the H(F)−H(H) distances are similar and fit to the tolerable 0.2−0.3 Å interval, the corresponding hydrogen atoms around the C2 atom in the K:DMSeO escaped from their positions to a distance of 0.6−0.7 Å. Such differences in the positions of the hydrogen atoms consequently led to the formation of the different hydrogen C−H···O bonds (see below).

Hydrogen bonds

In general, the calculated OH bond distances (Table 4) are in good agreement with the mean value

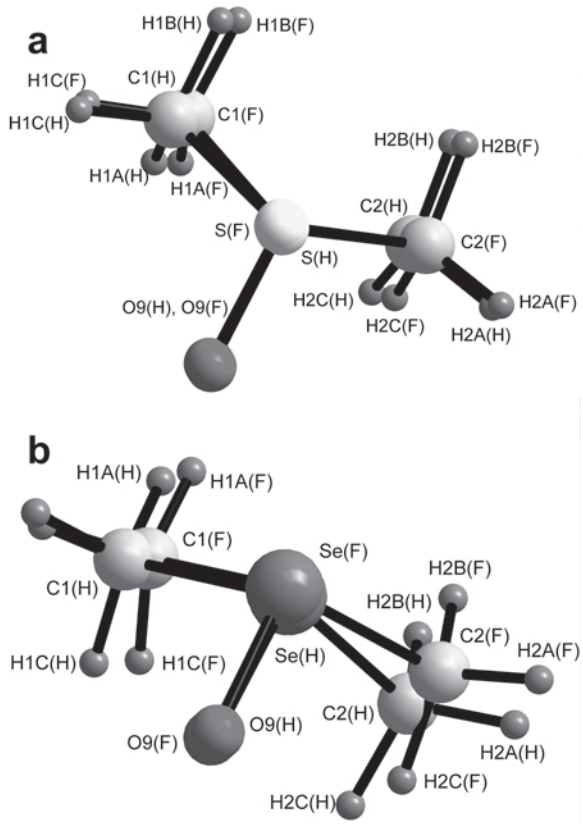

Figure 2. Overlay of the molecules optimized in the F and H computational models.

of 0.969(1) Å reported in the survey of the O–H···O hydrogen bond geometries (Ceccarelli *et al.*, 1981). Similarly, the O···O separations and the O–H···O bond angles obtained for both the K:DMSO and K:DMSeO intercalates are in reasonable agreement with the mean values of 2.77(7) Å and ~167º given in the above-mentioned survey. With the O–H···O bond angles close to the linearity and with the H···O separation of <2.2 Å, the strength of the hydrogen bonds in both structures can be ranked as 'moderately strong,' the nature of which is supposed to be electrostatic (Steiner, 2002). If taking the O···O separation as the measure of hydrogen bond strength, then the weakest (Figure 3a) are the bonds involving the H14 atoms and the strength of the bonds increases for the bonds involving the H12 and H13 hydrogen atoms.

If the intercalation is incomplete, as simulated by the computational H model, three hydroxyl groups lose their partners in the hydrogen bonds and reorient inside the interlayer space to reach the energy minimum (Figure 4). From the summary of angles formed by the individual OH bonds, with the reference plane fit through the hydroxyl oxygen atoms (Table 5), their variability is independent of the nature of the intercalating organic molecule. Assumed for the purpose of this study, though with a little caution, is that the unbonded hydroxyl groups behave like 'free' groups and contribute to the vibrational densities of states at different energies compared to those which are hydrogen-bonded. Note, however, that the (static) situation presented in Figure 4b,c probably represents only one of the possible minima and that the character of the changes in the Al–O–H angles is very dynamic in the real structure.

The stability of the K:DMSO and K:DMSeO structures is also supported by the C–H···O hydrogen bonds. The fundamental nature of this type of interaction (electrostatic or van der Waals) remains an open question (Desiraju, 1991) and this is especially true when they appear in such complex environments as the structures studied here. Although several studies of this type of contact have given somewhat contradictory results, the C–H···O interactions behave much like a more conventional O–H···O in most respects (*e.g.* Gu *et al.*, 1999; Steiner, 2002).

Taking into account the values of the C···O and H···O separations summarized in Table 4, the C–H···O bonds in the K:DMSO and K:DMSeO structures, on one hand, fall into the ranges expected for a weak bond. On the other hand, the bonds are so bent that they appear at the edge of the boundary of accepted values (Castellano, 2004). Variability in the C–H···O bond geometries in both intercalates is reflected by the formation of the bonds depending on the environment of the organic molecules (Figure 3b,c). This difference is so subtle that it is scarcely manifested in terms of changes in, for example, the vibrational spectra.

The most perplexing weak contacts in the structures analyzed are the O–H···S (Se) contacts, analysis of which cannot be routinely based on the accumulated data because the number of accurate crystal structures refined from low-temperature, single-crystal, neutron data is still too small (Steiner, 1998). This gap was recently partially filled by the computational study of the hydrogen-bond properties in sulfoxides and selenoxides (Renault and Le Questel, 2004) in which hydrogen bonds were found to be significantly stronger in the selenoxides even though the hydrogen-bond directionalities and linearities were similar. However, any thorough analysis of these contacts in the structures of K:DMSO and K:DMSeO would require a completely different computational approach (a higher level of the theory) and is beyond the scope of this study.

Calculated vibrational modes

A graphic comparison of the total vibrational density of states (DOS) based on the H computational models (Figure 5, the full lists of the calculated modes along with their assignments are in Appendices A and B) revealed mainly that the shapes of the spectra are similar, the most striking difference being the red shift of the doublet of the inner-surface OH stretching modes of the K:DMSeO relative to their counterparts in the K:DMSO. A minor difference was also recognized in the

Table 4. Hydrogen-bond parameters (Å, º) in the K:DMSO (upper) and the K:DMSeO (lower) intercalates. The values separated by oblique symbols are for the F and H computational models, respectively. Note that only the C−H···O bonds with C···O <3.5 Å are presented. The contacts recognized in the H model are given in italic type. The labels A−C in the rightmost column provide the links to the hydrogen bonds depicted in Figure 3b,c (D − donor, A − acceptor).

	D–H	H···A	D···A	D–H···A	Label
K:DMSO					
O12-H12...O9c	0.98	1.81	2.784	175	
O12c-H12c...O9^{i}	0.98	1.81/1.76	2.784/2.739	175/174	
O13-H13...O9^{ii}	0.98	1.82/1.81	2.797/2.784	175/175	
O13c-H13c...O9c	0.98	1.82	2.797	175	
O14-H14...O9c	0.97	1.96	2.932	179	
O14c-H14c...O9	0.97	1.96/1.94	2.932/2.912	179/178	
O12-H12...S1c^{i}	0.98	2.78/2.77	3.663/3.680	150/153	
O12c-H12c...S1^{i}	0.98	2.78	3.663	150	
O13-H13...S1^{ii}	0.98	2.86/2.83	3.735/3.696	150/148	
O13c-H13c...S1c	0.98	2.86	3.735	150	
C1-H1B···O5	1.09	2.56	3.337	127	A
C1c···H1Bc···O5c	1.09	2.56	3.337	127	
C1-H1B···O3c	1.09	2.53	3.308	127	B
K:DMSeO					
O12-H12...O9c^{i}	0.99	1.78	2.768	176	
O12c-H12c...O9^{i}	0.99	1.78/1.69	2.768/2.681	176/175	
O13-H13...O9^{ii}	0.98	1.74/1.75	2.717/2.728	175/175	
O13c-H13c...O9c	0.98	1.74	2.717	175	
O14-H14...O9c	0.97	1.88/1.88	2.848/2.849	177/175	
O14c-H14c...O9	0.97	1.88	2.848	177	
O12-H12...Se1c^{i}	0.99	2.76	3.579	141	
O12c-H12c...Se1^{i}	0.99	2.76/2.83	3.579/3.709	141/148	
O13-H13...Se1^{ii}	0.98	2.87/2.84	3.734/3.684	147/144	
O13c-H13c...Se1c	0.98	2.87	3.734	147	
C1-H1A···O5	1.08	2.56	3.297	124	A
C1-H1A···O3c	1.09	2.64	3.331	120	B
C1-H1B···O5c	1.09	2.65	3.412	126	C

Symmetry codes: (*i*) 1+*x*,*y*,*z*; (*ii*) 1+*x*,1+*y*,*z*; (*iii*) *x*,−1+*y*,1+*z*; (*iv*) *x*,*y*,1+*z*

shapes of the two bands in the ~2900−3200 cm^{-1} region assigned to the CH-stretching modes. Splitting of these bands (detailed in Figure 6) indicates that the bands situated at the higher energies belong to the CH-stretching modes of the methyl groups localized closer to the plane of the basal oxygen atoms, although the difference is rather subtle, ~17 cm^{-1} (K:DMSO) and ~40 cm^{-1} (K:DMSeO). Such a splitting, indicating differentiation of the methyl groups, was documented experimentally by the time development of the shape of the Raman spectra of a K:DMSO intercalate during intercalation (Johnston *et al*., 1984). A comparison of the energies of the calculated and the measured modes shows that the most intense peak in the Raman spectra (2919 cm^{-1}) corresponds to the concerted CH-stretching movement in both methyl groups, while the rest of the measured peaks were assigned to the individual stretching modes. Splitting of these CH modes was also

Table 5. The angles of the O−H bonds formed with the plane fit to oxygen atoms of the inner-surface hydroxyl groups (º) in the K:DMSO and K:DMSeO intercalates. The letters F and H indicate the respective computational models.

	K:DMSO		K:DMSeO	
Bond	F	H	F	H
O11−H11,	2 × 2.7	9.6	2 × 1.9	10.1
O11c−H11c		6.7		5.6
O12−H12,	2 × 47.6	51.4	2 × 42.9	31.0
O12c−H12c		50.5		48.2
O13−H13,	2 × 47.5	44.9	2 × 47.1	43.0
O13c−H13c		82.4		79.0
O14−H14,	2 × 41.3	12.5	2 × 39.8	17.3
O14c−H14c		42.2		43.1

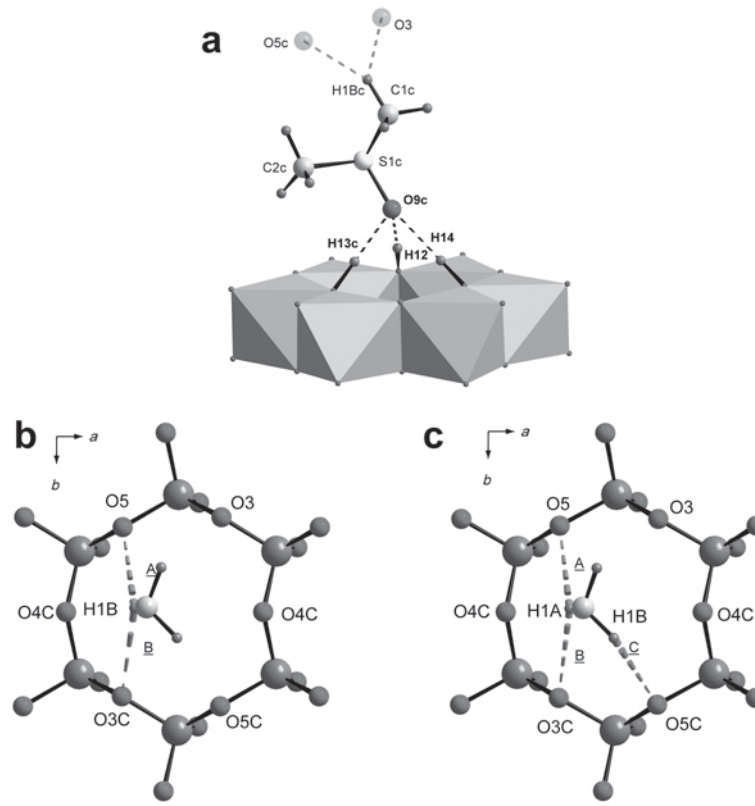

Figure 3. (a) Hydrogen bonds formed by three OH groups and the intercalating molecule. Two possible contacts to the adjacent tetrahedral sheet are shown in faint colors. For the sake of clarity, only the interacting OH bonds are depicted. Possible C-H···O hydrogen bonds in the K:DMSO and K:DMSeO intercalates are displayed in parts (b) and (c). The underlined letters A, B, and C indicate links to Table 4.

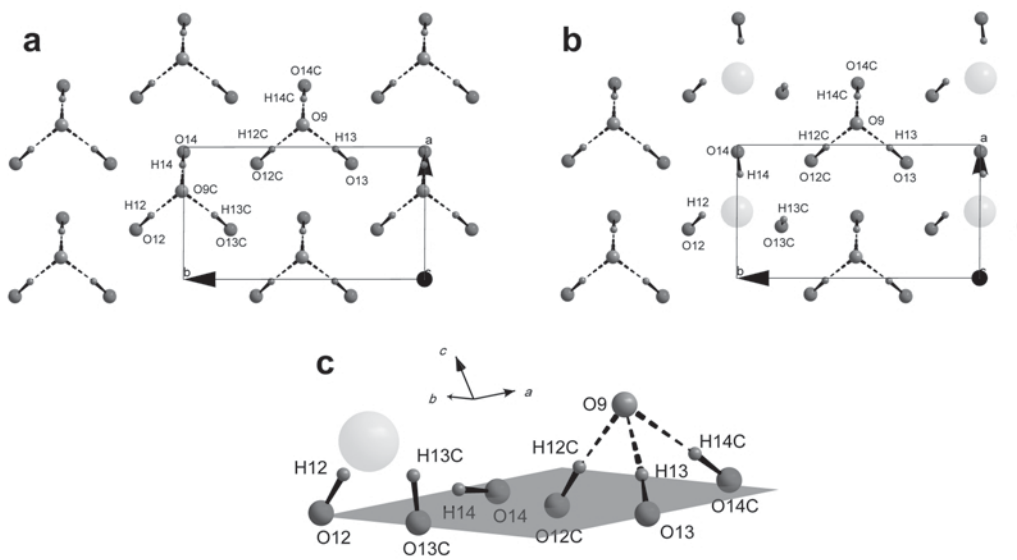

Figure 4. Orientation of the inner-surface OH bonds in the F (a) and H (b) computational models shown in the projection along the *c* axis. Light-gray circles indicate the missing organic molecules. (c) Mutual orientation of the selected OH bonds and the reference plane fit through O12−O14.

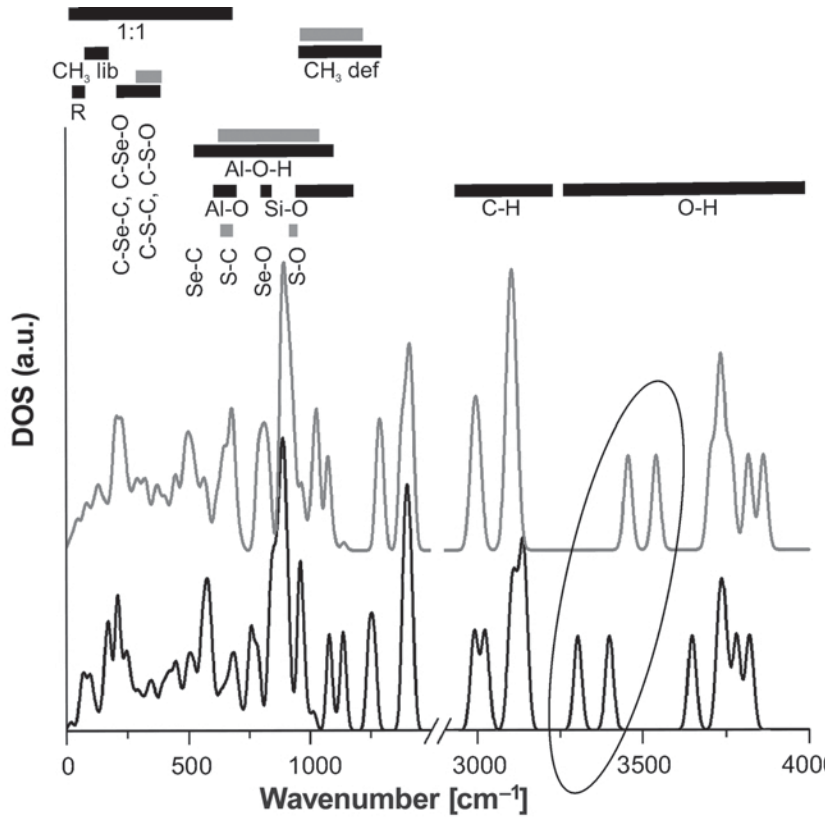

Figure 5. Calculated total vibrational density of states (DOS) for K:DMSO (upper spectrum) and K:DMSeO (lower spectrum). The regions with the most important vibrational modes are indicated on the top in black (K:DMSeO) and gray (K:DMSO), the individual C-H and O-H stretching regions overlap. R – region of rocking movement of the molecules. The largest shift in the OH-stretching modes is marked by the ellipse.

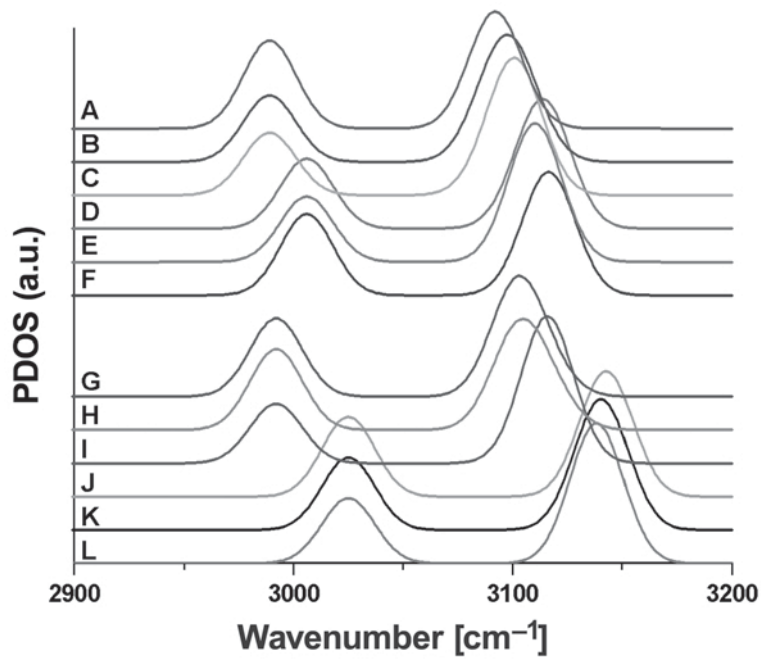

Figure 6. Partial vibrational density of states (PDOS) showing the contributions of the CH stretching modes to the vibrational spectra. The curves A–C (G–I) and D–F (J–L) represent the contributions of the C2-H2C, -H2B, -H2A, and C1-H1C, -H1B, -H1A stretching modes to the spectra of K:DMSO (K:DMSeO), respectively.

recognized in the K:DMSeO spectrum (figure 5 of the RBT study). The experimentally determined wavenumbers were between 2920 and 3041 cm^{-1}, which is in good agreement with the calculated values of 2902–3048 cm^{-1} (Appendix B).

The detailed OH-stretching modes (Figure 7) highlight the insensitivity to the environment of the energy of the modes deriving from the inner OH group, in accordance with the empirical experience accumulated from the analyses of different samples of kaolinites and/or their intercalates mentioned above. As expected, the formation of the O–H···O hydrogen bonds involving the inner-surface hydroxyl groups caused red shifts (to smaller wavenumber) of the positions of the peaks. The overall trends in the shifts correlate directly with the strengths of the respective hydrogen bonds measured through the O···O separation (Table 4). Because the Se=O bond is more polar than the S=O bond, the red shifts are noticeably larger in the case of K:DMSeO. Formation of the weakest O–H···O hydrogen bond in the K:DMSO intercalate involving H14c is thus reflected by the shift of only 59 cm^{-1}, but with further shortening of the O···O contacts, it grows to 278 cm^{-1} (H13) and 407 cm^{-1} (H12c). In the case of K:DMSeO, the order of the shifts is preserved, but the respective values are substantially larger, in accordance with the smaller O···O separations, 135, 481, and 537 cm^{-1}, respectively. Also evident is that the OH modes appearing between 3200 and 3600 cm^{-1} are not pure modes (Figure 7), but

Table 6. Summary of the calculated and the experimentally observed (A–D) wavenumbers (cm^{-1}) of the OH-stretching modes in the K:DMSO intercalate. Note that in the leftmost column, both unscaled and scaled (in parenthesis) values are given.

This work	A	B	C	D
3864 (3742) O12-H12 3820 (3700) O13c-H13c 3766 (3647) O14-H14	3690, 3664, 3646, 3617	3695, 3668, 3652	3650, 3670, 3684, 3693	3693
3738 (3620) O11-H11 3735 (3617) O11c-H11c	3620	3620	3620	3620
3707 (3590) O14c-H14c 3542 (3430) O13-H13 3458 (3349) O12c-H12c	3658, 3535, 3499	3538 3502	3660, 3536, 3501	3665
Calc	IR	Raman	Raman	Raman

(A) Olejnik *et al*. (1968); (B) Johnston *et al*. (1984); (C) spectrum collected at 298 K, Frost *et al*. (2000); (D) Martens *et al*. (2002).

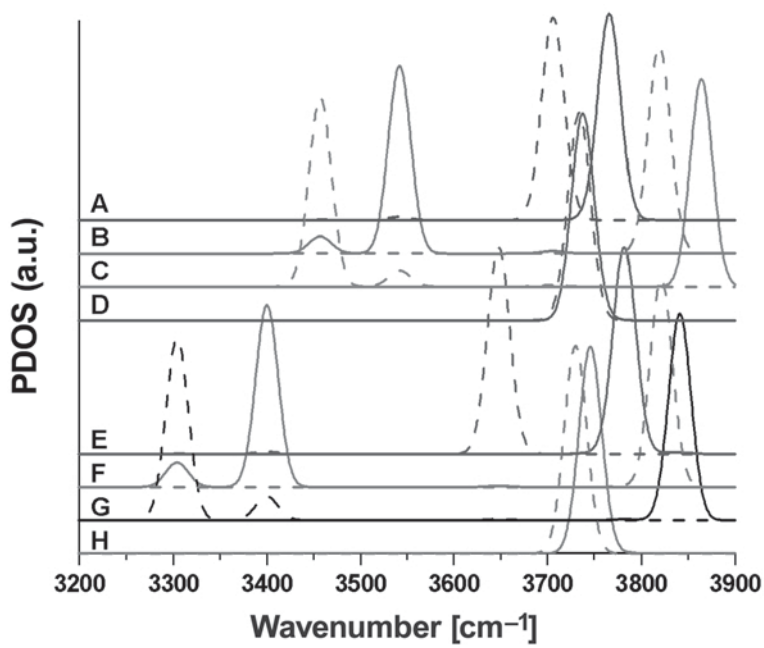

Figure 7. Partial vibrational density of states (PDOS) detailing the contributions of the individual OH-stretching modes. The upper quadruplet of the curves shows the contributions to the K:DMSO spectrum, while the lower shows the contributions the K:DMSeO spectrum. The curves at the A and E levels depict the contributions of the O14-H14 (solid lines) and the O14c-H14c (dashed lines) stretching vibrations. Analogously, the traces at B and F levels stand for the contributions of O13-H13/O13c-H13c, C(G) of the O12-H12/O12c-H12c, and the D(H) pair of those from O11-H11/O11c-H11c stretching vibrations, respectively.

have major and minor components which are inseparable experimentally.

Experimentally determined and calculated OH-stretching modes (Figure 8) in the K:DMSO intercalate were compared (Table 6) and differences were found. Some of the discrepancies can be explained by the computational method, which tends to overestimate the energies of the modes, and were partially overcome by scaling the spectra by multiplying by 0.968. This constant was obtained by comparison of the experimentally determined and calculated energy for the inner OH-stretching mode. This mode was found to be stable both experimentally and theoretically. Any complete reconciliation of the observed and calculated modes is, however, limited by the fact that the experimentally collected spectra evidently depend on the order in the parent kaolinite structures, while the calculated modes have been derived from the perfectly ordered structure.

While the OH-stretching modes in the K:DMSO intercalate have been the subject of several studies, the same modes in the K:DMSeO are documented only by the IR spectrum in the RBT study. The dominant feature in this spectrum is a very broad asymmetric maximum spanning over ~400 cm^{-1}. On its low-energy tail

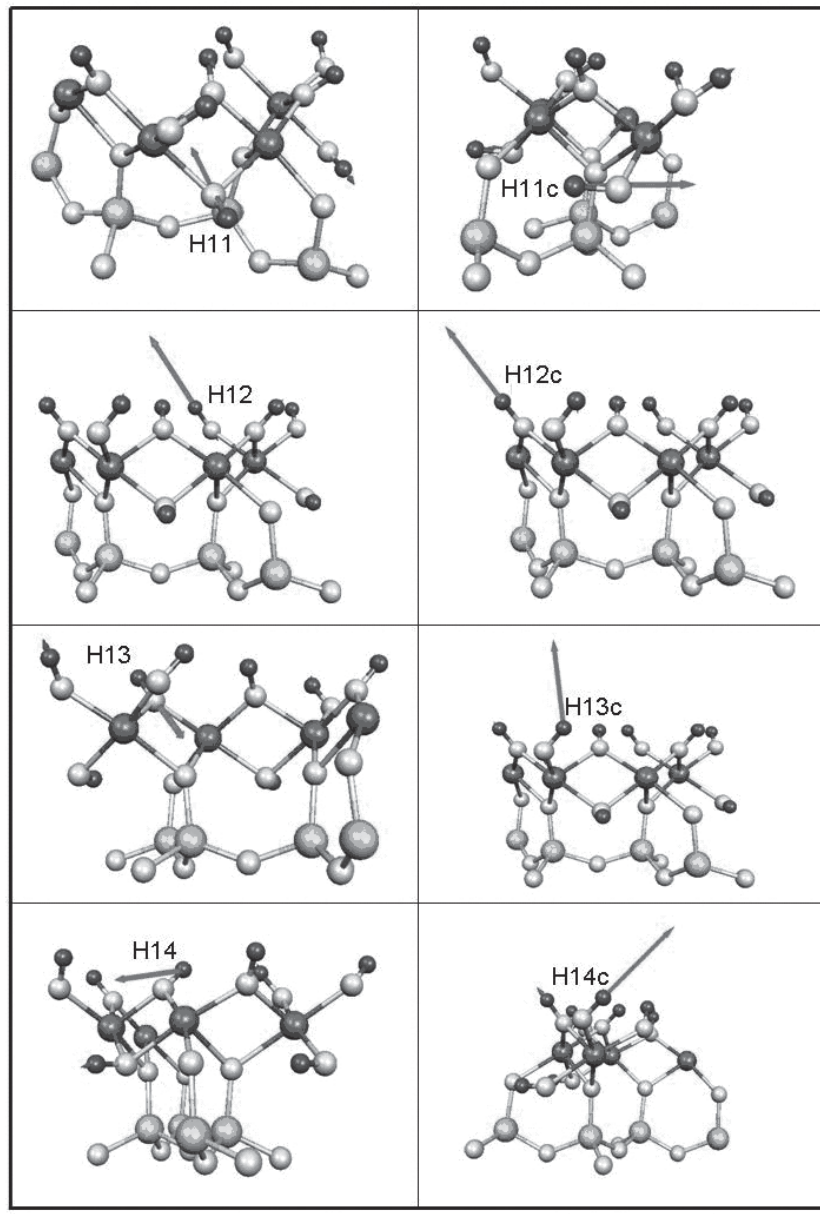

Figure 8. Visualization of the dominant OH modes in the K:DMSO structure. Because the orientations of the modes in the K:DMSeO are very similar, they are not shown. Prepared by the *Molekel* program of Portmann and Luthi (2000).

(3100−2800 cm^{-1}), several sharp and well separated peaks are superimposed, which can (using Appendix B) be assigned to CH-stretching modes. Considering the order of the modes in Appendix B, the broad feature centered at ~3388 cm^{-1} hides the stretching modes of the OH groups involved in the hydrogen bonds. The most intense, sharp peak in the spectrum (~3616 cm^{-1}) is, by experience, assigned to stretching movement of the inner-OH groups. Finally, comparison of the positions of the peak reported in the RBT paper for a 'well-crystalline kaolinite' at 3694 cm^{-1} with that at 3689 cm^{-1}, and also with the energies calculated for 'free' OH groups in the structure of the K:DMSeO (Appendix B), lead to the suggestion that this peak represents all non-hydrogen bonded OH groups.

Whereas the stretching modes are of primary interest with respect to the routine characterization of the hydrogen bonds in the kaolinite intercalates by photon spectroscopies, this is not always the case for Al−O−H bending vibrational modes. This is because these modes

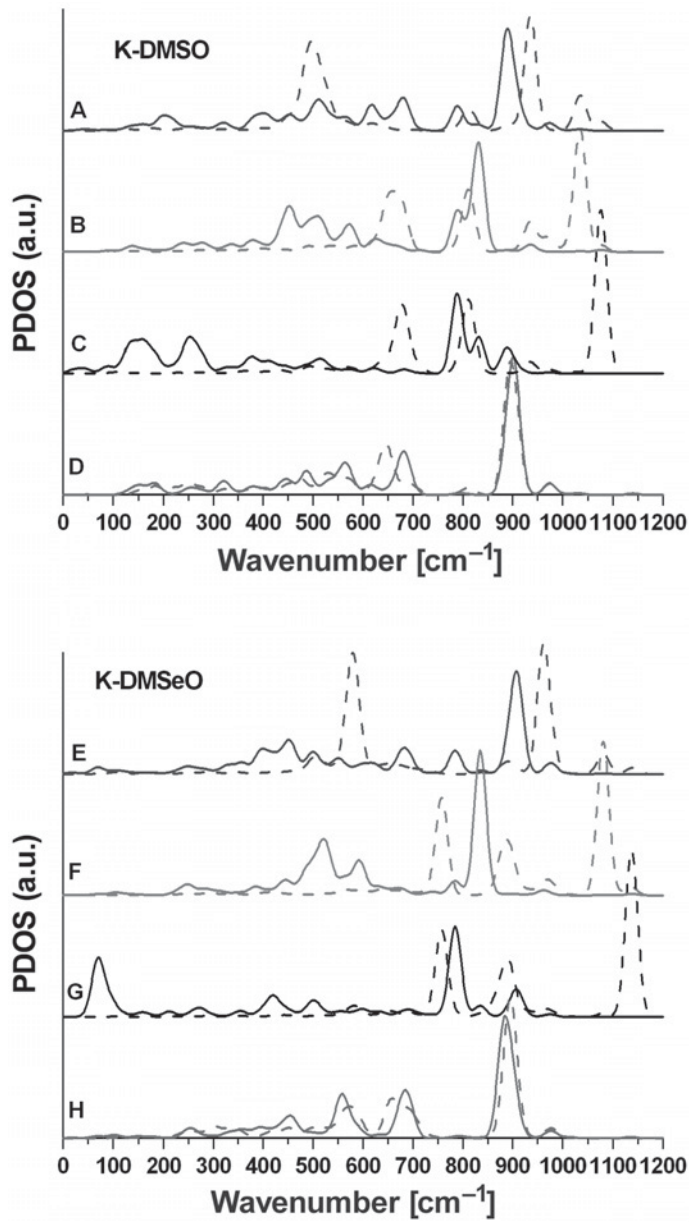

Figure 9. Partial vibrational density of states (PDOS) detailing the contributions of the individual OH bending modes: (a) K:DMSO spectrum; (b) K:DMSeO spectrum. The curves at the A and E levels depict the contributions of the O14-H14 (solid lines) and the O14c-H14c (dashed lines) bending vibrations. Analogously, the traces at B and F levels stand for the contributions of O13-H13/O13c-H13c, C(G) of the O12-H12/O12c-H12c, and the D(H) pair of those from O11-H11/O11c-H11c bending vibrations, respectively.

are masked by the vibrational modes originating from the stretching movements of the bonds linking the atoms forming either the 1:1 layer or the organic molecules (Figure 5). Moreover, these modes could be compared to the stretching modes, distributed over the larger intervals of energies, which make their identification difficult unless hydrogen-sensitive vibrational spectroscopy based on inelastic neutron scattering (INS) is used.

An impression of the degree of complexity of these modes can be gained from Figure 9 and from Appendices A and B. It is evident that although the modes are spread over the wide intervals of energies, the most important features are concentrated between ~800 and 1200 cm^{-1}. The exception that proves the rule are the modes reflecting the movements of the H12 atoms (Figure 9, traces C and G) since they both show non-negligible contributions to the total vibrational density of states even below 300 cm^{-1}. If focusing only on the dominant features in Figure 9, it is seen that the well separated modes appearing on the top of the depicted energy range reflect the movements of the hydrogen atoms involved in the hydrogen bonds (Figure 4). This increase in the energy (blue shift) relative to the energies of the 'free-OH' vibrational modes correlates with the strength of the respective hydrogen bonds measured through the individual O···O separations (Table 4). In contrast, the vibrational modes related to the OH groups not involved in hydrogen bonds are concentrated in a much smaller space and it will be, therefore, rather difficult to separate in the experimental spectra. The behavior of the modes corresponding to the bending movements of inner hydroxyl groups OH11/OH11c (Figure 9, traces D and H) is very interesting. Although they enjoy fewer degrees of freedom for their movement than the inner-surface hydroxyls, the spectra they produce are comparable, in terms of their complexity, with the others. Looking more closely at the bending modes in the spectra, the complexity is assumed to arise also from a modulation of the changes of the Al−O−H angles by a slower deformation movement of the entire 1:1 layer.

The regions between 900 and 1150 and between 600 and 800 cm^{-1} in the K:DMSO intercalate were documented by Johnston *et al*. (1984). One asymmetric broad peak (1024 cm^{-1}) and one sharper (955 cm^{-1}) peak are interpreted as a possible mixture of S=O and Si−O stretching and Al−O−H bending modes together with the methyl-group deformation modes (Appendix A). The peaks in the lower-energy range are assigned to both symmetric and asymmetric C−S and Al−O stretching as well as to the O−Si−O and Al−O−H bending modes. The modes appearing within 1270−1418 cm^{-1} in the K:DMSeO spectrum in the RBT study are all methyl-group deformation modes. The group of three, broad, overlapping peaks between 736 and 831 cm^{-1} (figure 7b of the RBT work) consists mainly of Al−O−H bending modes with smaller contributions of CH_3 bending, and Si−O and Se=O stretching modes (Appendix B).

ACKNOWLEDGMENTS

The authors acknowledge financial support from the Slovak Research and Development Agency APVV under contract APVV-51-050505. This work benefited from the 'Centers of Excellence' program of the Slovak Academy of Sciences (COMCHEM, Contract no. II/1/2007).

REFERENCES

Balan, E., Marco Saitta, A., Mauri, F., and Calas, G. (2001) First-principles modelling of the infrared spectrum of kaolinite. *American Mineralogist*, **86**, 1321−1330.

Balan, E., Marco Saitta, A., Mauri, F., Lemaire, C., and Guyot, F. (2002) First-principles calculations of the infrared spectrum of lizardite. *American Mineralogist* **87**, 1286−1290.

Blöchl, P.E., (1994) Projector augmented-wave method. *Physical Review B*, **50**, 17953−17979.

Brandenburg, K. (2006) *Diamond.*. Version 3.1d. Crystal Impact GbR, Bonn, Germany.

Bylander, D.M., Kleinman, L., and Lee, S. (1990) Self-consistent calculations of the energy bands and bonding properties of B-12(C-3). *Physical Review* B, **42**, 1394−1403.

Castellano, R.K. (2004) Progress toward understanding the nature and function of C-H···O interactions. *Current Organic Chemistry*, **8**, 845−865.

Ceccarelli, C., Jeffrey, G.A., and Taylor, R. (1981) A survey of O-H···O hydrogen bonds geometries determined by neutron diffraction. *Journal of Molecular Structure*, **70**, 255−271.

Desiraju, G.R. (1991) The C-H···O hydrogen bond in crystals: what is it? *Accounts of Chemical Research*, **24**, 290−296.

Dobado, J.A., Martinez-Garcia, H., Molina, J.M., and Sundberg, M.R. (1999) Chemical bonding in hypervalent molecules revised. 2. Application of the atoms in molecules theory to Y_2XZ and Y_2XZ_2 (Y=H, F, CH_3; X=O, S, Se; Z=O,S) compounds. *Journal of the American Chemical Society*, **121**, 3156−3164.

Fang, Q., Huang, S., and Wang, W. (2005) Intercalation of dimethysulfoxide in kaolinite: molecular dynamics study. *Chemical Physics Letters*, **411**, 233−237.

Filatov, A.S., Block, E., and Petrukhina, M.A. (2005) Dimethyl selenoxide. *Acta Crystallographica*, C**61,** 596−598.

Frost, R.L., Kristof, J., Horvath, E., and Kloprogge, J.T. (2000) Kaolinite hydroxyls in dimethylsulfoxide-intercalated kaolinites at 77K − a Raman spectroscopic study. *Clay Minerals*, **35**, 443−454.

Gu, Y., Kar, T., and Scheiner, S. (1999) Fundamental properties of the C-H···O interaction: is it a true hydrogen bond? *Journal of the American Chemical Society*, **121**, 9411−9422.

Hafner, J. (2003) Vibrational spectroscopy using ab initio density-functional techniques. *Journal of Molecular Structure*, **651**−**653**, 3−17.

Hayashi, S. (1995) NMR study of dynamics of dimethyl sulfoxide molecules in kaolinite/dimethyl sulfoxide intercalation compounds. *Journal of Physical Chemistry*, **99**, 7120−7129.

Hayashi, S. (1997) NMR study of dynamics and evolution of guest molecules in kaolinite /dimethyl sulfoxide intercalation compounds. *Clays and Clay Minerals*, **45**, 724−732.

Hobbs, J.D., Cygan, R.T., Nagy, K.L., Schultz, P.A., and Sears, M. (1997) All-atom ab initio energy minimization of the kaolinite structure. *American Mineralogist*, **82**, 657−662.

Ibberson, R.M. (2005) Neutron powder diffraction studies of

dimethyl sulfoxide. *Acta Crystallographica*, **C61**, 571–573.

Johnston, C.T., Sposito, G., Bocian, D.F., and Birge, R.R. (1984) Vibrational spectroscopic study of the interlamellar kaolinite-dimethylsulfoxide complex. *Journal of Physical Chemistry*, **88**, 5959–5964.

Kirkpatrick, R.J., Kalinchev, A.G., Wang, J., Hou, X., and Amonette, J. (2005) Molecular modeling of the vibrational spectra of interlayer and surface species of layered double hydroxides. Pp. 239–285 in: *The Application of Vibrational Spectroscopy to Clay Minerals and Layered Double Hydroxides* (J.T. Kloprogge, Editor). CMS Workshop Lecture Series, **13**, The Clay Minerals Society, Aurora, CO, USA.

Kresse, G. and Furthmüller, J. (1996a) Efficient iterative scheme for ab initio total energy calculations using a plane-wave basis set. *Physical Review B*, **54**, 11169–11186.

Kresse, G. and Furthmüller, J. (1996b) Efficiency of ab-initio total energy calculations for metals and semiconductors using a plane-wave basis set. *Computational Materials Science*, **6**, 15–50.

Kresse, G. and Hafner, J. (1993) Ab initio molecular dynamics for open-shell transition metals. *Physical Review B*, **48**, 13115–13118.

Kresse, G. and Hafner, J. (1994) Norm-conserving and ultrasoft pseudopotentials for first-row and transition elements. *Journal of Physics: Condensed Matter*, **6**, 8245–8527.

Kresse, G. and Joubert, J. (1999) From ultrasoft potentials to the projector augmented wave method. *Physical Review B*, **59**, 1758–1775.

Martens, W.N., Frost, R.L., Kristof, J., and Horvath, E. (2002) Modification of kaolinite surfaces through intercalation with deuterated dimethylsulfoxide. *Journal of Physical Chemistry*, **B106**, 4162–4171.

Michalková, A. and Tunega, D. (2007) Kaolinite, dimethylsulfoxide intercalate – a theoretical study. *Journal of Physical Chemistry*, **C111**, 11259–11266.

Neder, R.B., Burghammer, M., Grasl, Th., Schulz, H., Bram, A., and Fiedler, S. (1999) Refinement of the kaolinite structure from single crystal synchrotron data. *Clays and Clay Minerals*, **47**, 487–494.

Olejnik, S., Aylmore, L.A.G., Posner, A.M., and Quirk, J.P. (1968) Infrared spectra of kaolin mineral-dimethylsulfoxide complexes. *The Journal of Physical Chemistry*, **72**, 241–249.

Olejnik, S., Posner, A.M., and Quirk, J.P. (1970) The intercalation of polar organic compounds into kaolinite. *Clay Minerals*, **8**, 421–434.

Perdew, J.P. and Wang, Y. (1992) Accurate and simple analytic representation of the electron-gas correlation energy. *Physical Review*, **B45**, 13244–13249.

Perdew, J.P. and Zunger, A. (1981) Self-interaction correction to density-functional approximations for many-electron systems. *Physical Review*, **B23**, 5048–5079.

Portmann, S. and Luthi, H.P. (2000) MOLEKEL: an interactive molecular graphics tool, *Chimia*, **54**, 766–769.

Raupach, M., Barron, P.F., and Thompson, J.G. (1987) Nuclear magnetic resonance, infrared, and X-ray powder diffraction study of dimethylsulfoxide and dimethylselenoxide intercalates with kaolinite. *Clays and Clay Minerals*, **35**, 208–219.

Renault, E. and Le Questel, J.-Y. (2004) Selenoxides are better hydrogen-bond acceptors than sulfoxides: a crystallographic database and theoretical investigation. *Journal of Physical Chemistry*, **A108**, 7232–7240.

Smrčok, L'. (1995) A comparison of powder diffraction studies of kaolin group minerals. *Zeitschrift für Kristallographie*, **210**, 177–183.

Spek, A.L. (2002) *PLATON. A Multipurpose Crystallographic Tool*. Utrecht University, The Netherlands. (www.cryst.chem.uu.nl/platon).

Steiner, T. (1998) Lengthening of the covalent X–H bond in heteronuclear hydrogen bonds quantified from organic and organometalic neutron crystal structures. *Journal of Physical Chemistry*, **A102**, 7041–7052.

Steiner, T. (2002) The hydrogen bond in the solid state. *Angewandte Chemie – International Edition*, **41**, 48–76.

Teter, M.P., Payne, M.C., and Allan, D.C (1989) Solution of Schrodinger's equations for large systems. *Physical Review*, **B40**, 12255–12263.

Thompson, J.G. and Cuff, C. (1985) Crystal structure of kaolinite:dimethylsulfoxide intercalate. *Clays and Clay Minerals*, **11**, 490–500.

(*Received 14 April 2008; revised 24 September 2008; Ms. 0096; A.E. S. Petit*)

APPENDIX A

Unscaled vibrational modes [cm^{-1}] in the kaolinite:DMSO intercalate calculated using the H model. The dominant modes in certain groups are in bold type.

Wavenumber [cm^{-1}]	Type of vibrational mode
3864	O12−H12 stretch
3820	O13c−H13c stretch
3766	O14−H14 stretch
3738	O11−H11 stretch
3735	O11c−H11c stretch
3707	O14c−H14c stretch
3542	**O13−H13,** O12c−H12c symmetric stretch
3458	**O12c−H12c,** O13−H13 asymmetric stretch
3117	C1−H1A, C1−H1C asymmetric stretch
3110	C1−H1C, C1−H1B asymmetric stretch
3102	C2−H2A, C2−H2B asymmetric stretch
3092	C2−H2C, C2−H2B asymmetric stretch
3007	C1−H1A, C1−H1B, C1−H1C symmetric stretch
2990	C2−H2A, C2−H2B, C2−H2C symmetric stretch
1423	H−C−H scissoring
1413	
1398	
1377	Methyl-group out-of-plane deformation
1300	
1282	
1141	Si−O basal asymmetric stretch
1100	Si−O basal asymmetric stretch
1094	Si−O basal symmetric stretch
1077	Al1c−O12c−H12c bending
1035	Al2−O14c−H14c bending, **Al2−O13−H13 bending**
1025	Si−O apical symmetric stretch, C−S−C bending
1022	Si−O basal asymmetric stretch
1016	Si−O apical symmetric stretch, methyl-group out-of-plane bending
999	Si−O basal asymmetric stretch
997	Si−O basal asymmetric stretch
975	Si−O apical asymmetric stretch, Al−O−H bending
964	S−O9 stretch, methyl-group out-of-plane deformation, Si−O apical symmetric stretch
936	Al2−O14c−H14c bending
929	Si−O apical asymmetric stretch
922	S−O9 stretch, **methyl-group (C1) out-of-plane deformation**
918	S−O9 stretch, **methyl-group (C2) out-of-plane deformation**
910	**Al−O−H (inner) bending, Al2−O12−H12 bending,** methyl-group (C2) wagging
902	Al−O−H (inner) bending
891	Al2c−O14−H14 bending, Al−O−H (inner) bending
889	Methyl-group out-of-plane deformation
886	Al1−O14−H14 bending, Al2c−O11−H11 bending
833	**Al2c−O13c−H13c bending,** Al2−O12−H12 bending
814	Al1c−O12c−H12c bending, Al2−O13−H13 bending
806	Si−O basal asymmetric stretch, Al1c−O12c−H12c bending, Al2−O13−H13 bending
795	Si−O basal asymmetric stretch
789	**Al1−O14−H14 bending**, Al2−O12−H12 bending, Al2c−O13c−H13c bending
779	Si−O basal asymmetric stretch
713	1:1 layer deformation
698	Si−O basal asymmetric stretch
688	**S−C asymmetric stretch**, Al2c−O12c−H12c, Al2−O13−H13 bending, Si−O symmetric stretch
685	Al−O−H bending, S−C asymmetric stretch
683	**Al−O asymmetric stretch,** S−C asymmetric stretch, O−Si−O bending
674	Al−O−H bending, O−Si−O bending
654	S−C symmetric stretch, Al−O asymmetric stretch, O−Si−O bending
647	**S−C symmetric stretch,** Al−O−H bending

Wavenumber [cm^{-1}]	Type of vibrational mode
640	S−C2 stretch, Al−O−H bending
623	
621	
610	
585	
575	
563	
559	
552	Octahedral sheet deformation
538	
531	
527	
515	
512	
504	
498	
492	
486	
476	
455	
449	
443	
438	
435	1:1 layer deformation
417	
410	
405	
404	
400	
387	
380	
375	C−S−O bending, 1:1 layer deformation
364	C−S−O bending, 1:1 layer deformation
358	1:1 layer deformation
344	1:1 layer deformation
338	C−S−C wagging, 1:1 layer deformation
333	1:1 layer deformation
327	C−S−O bending, 1:1 layer deformation
322	C−S−O bending, 1:1 layer deformation
321	**C−S−O bending**, 1:1 layer deformation
316	C−S−O bending, 1:1 layer deformation
301	
299	
295	1:1 layer deformation
283	
279	C−S−C bending, 1:1 layer deformation
275	1:1 layer deformation
271	1:1 layer deformation
260	methyl-group (C2) libration, 1:1 layer deformation
250	1:1 layer deformation
248	methyl-group libration (**C2**), 1:1 layer deformation
237	methyl-group libration, 1:1 layer deformation
231	methyl-group libration (**C2**)
225	1:1 layer deformation, methyl-group libration
220	1:1 layer deformation, methyl-group (C2) libration
206	methyl-group libration
201	1:1 layer deformation, methyl-group libration
198	O−Al−O wagging, methyl-group libration
185	Al−O−H bending
180	1:1 layer deformation

Wavenumber [cm^{-1}]	Type of vibrational mode
162	**Al2−O12−H12 bending**, methyl-group (C2) libration, 1:1 layer deformation
153	octahedral sheet deformation
139	octahedral sheet deformation
136	1:1 layer deformation, DMSO rocking
132	1:1 layer deformation
125	1:1 layer deformation, DMSO rocking
118	
108	Methyl-group (C1) libration, octahedral-sheet deformation
92	DMSO rocking, Al2−O12−H12 bending
89	DMSO rocking, 1:1 layer deformation
76	DMSO rocking
54	DMSO rocking, 1:1 layer deformation
42	
19	
9	Translation along *y*

APPENDIX B.

Unscaled vibrational modes [cm^{-1}] in the kaolinite:DMSeO intercalate calculated using the H model. The dominant modes in certain groups are in bold type.

Wavenumber [cm^{-1}]	Type of vibrational mode
3842	O12−H12 stretch
3821	O13c−H13c stretch
3783	O14−H14 stretch
3746	O11−H11 stretch
3731	O11c−H11c stretch
3648	O14c−H14c stretch
3400	**O13−H13**, O12c−H12c symmetric stretch
3305	**O12c−H12c**, O13−H13 asymmetric stretch
3143	C1−H1B, C1−H1C asymmetric stretch
3139	C1−H1A, C1−H1B asymmetric stretch
3117	**C2−H2A**, C2−H2B asymmetric stretch
3103	C2−H2B, C2−H2C asymmetric stretch
3026	C1−H1A, C1−H1B, C1−H1C symmetric stretch
2992	C2−H2A, C2−H2B, C2−H2C symmetric stretch
1420	H−C−H scissoring
1409	Methyl-group out-of-plane deformation
1398	
1387	
1265	
1244	
1139	**Al1c−O12c−H12c bending**, Si−O basal asymmetric stretch
1134	Al2c− O12c−H12c bending Si−O basal asymmetric stretch
1111	Si−O basal asymmetric stretch
1082	Si−O basal symmetric stretch, **Al1−O13−H13 bending**
1081	
1019	Si−O basal asymmetric stretch
1014	Si−O apical symmetric stretch
1010	Si−O basal, apical asymmetric stretch
981	Al−O−H bending, Si−O basal, apical asymmetric stretch
976	Al−O−H bending, Si−O basal, apical asymmetric stretch
962	Al1c−O14c−H14c bending
959	Methyl-group out-of-plane deformation
931	Si−O apical asymmetric stretch, Al−O−H bending
912	Si−O apical asymmetric stretch, **Al1−O14−H14 bending** Al1c−O11c−H11c bending, Al2c−O11−H11 bending
902	**Si−O apical asymmetric stretch, Al−O−H bending,** methyl(C1) out-of-plane deformation
897	
892	Si−O apical asymmetric stretch**, Al−O−H bending, methyl(C1) out-of-plane deformation**

Wavenumber [cm^{-1}]	Type of vibrational mode
882	Si−O apical asymmetric stretch**,** Al−O−H bending**, Al−O−H (inner) bending**, methyl-group out-of-plane deformation
879	**Methyl-group out-of-plane bending, Al1c−O12c−H12c, Al2−O13−H13 bending**, Al1−O11−H11 bending
862	methyl-group out-of-plane bending
850	methyl-group out-of-plane bending
836	Al1c−O13c−H13c bending
806	1:1 layer deformation
794	Si−O basal asymmetric stretch
785	**Al1−O12−H12 bending,** Al1c−O13c−H13c bending
778	Si−O basal asymmetric stretch, Al−O−H bending
758	**Al1−O13−H13 bending,** Al2c−O12c−H12c bending
739 717	Se−O9 stretch, octahedral sheet deformation
701	1:1 layer deformation
696	Al−O asymmetric stretch
688	Al−O−H bending, O−Si−O bending, **Al1−O11−H11 bending**
675	Al−O−H bending, O−Si−O bending, **Al−O−H (inner) bending**
655	Al−O−H bending, O−Si−O bending, **Al1c−O11c−H11c bending**
640	Al−O asymmetric stretch
632 622 604	Octahedral sheet deformation
594	Al−O asymmetric stretch
587	Octahedral sheet deformation, Se−C1 stretch
583	Se−C asymmetric stretch, Al1c−O14c−H14c, Al1c−O11c−H11c bending
578	Se−C1 stretch, Al1c−O14c−H14c, Al1c−O11c−H11c bending
567	Se−C2 stretch, octahedral-sheet deformation
563	1:1 layer deformation
560	Se−C2 stretch, Al−O−H bending
556	1:1 layer deformation
549	1:1 layer deformation
527	Al1c−O13c−H13c bending
526 512 507 502 496 486 472 458 452 448 441 438 422 421 416 411 397 395 385 381	1:1 layer deformation
365	1:1 layer deformation, C2−Se−O9 bending
359 352	1:1 layer deformation, C1−Se−O9 bending
349	1:1 layer deformation, C2−Se−O9 bending
340 338	1:1 layer deformation, C−Se−O bending
328	1:1 layer deformation
316	1:1 layer deformation, C2−Se−O9 bending
309 299	C1−Se−C2 wagging, 1:1 layer deformation

Wavenumber [cm^{-1}]	Type of vibrational mode
298	1:1 layer deformation
289	1:1 layer deformation
284	C1−Se−C2 wagging, 1:1 layer deformation
274	
262	C1−Se−C2 bending, 1:1 layer deformation
258	
253	C1−Se−C2 wagging, 1:1 layer deformation
250	
246	C1−Se−C2 bending, 1:1 layer deformation
240	
228	Octahedral-sheet deformation, C1−Se−C2 wagging
212	**C1−Se−C2 bending**
210	**Methyl-group (C2) libration**
180	**Methyl-group (C1) libration**, 1:1 layer deformation
178	DMSeO rocking, 1:1 layer deformation
173	**Methyl-group (C1) libration**
161	Methyl-group libration in phase
149	1:1 layer deformation, methyl-group (C1) libration
130	1:1 layer deformation, C1−Se−C2 bending
117	1:1 layer deformation, methyl-group (C2) libration
107	1:1 layer deformation, methyl-group (C1) libration
102	DMSeO rocking, 1:1 layer deformation
94	Methyl-group (C1) libration, Al1−O12−H12 bending, DMSeO rocking
71	DMSeO rocking, **Al1−O12−H12 bending**
59	DMSeO rocking
18	DMSeO rocking, 1:1 layer deformation
17	DMSeO rocking, 1:1 layer deformation